RevMexAA (Serie de Conferencias), **36**, CD243–CD251 (2009)

POWER SPECTRA AND DENSITY PROBABILITY DISTRIBUTION FUNCTIONS IN SUPERSONIC HYDRODYNAMIC AND MHD TURBULENCE

M. N. Lemaster[1] and J. M. Stone[1]

RESUMEN

Presentamos un análisis del espectro de potencias y las funciones de distribución de probabilidad (PDFs por sus siglas en inglés) de la densidad de masa en simulaciones de turbulencia supersónica, hidrodinámica y MHD con propiedades acorde con nubes moleculares. Para este estudio utilizamos Athena, un nuevo código Godunov de orden superior. Encontramos que una resolución de 512^3 es insuficiente para resolver el rango inercial para el espectro de potencias de la velocidad. Resoluciones mucho más altas son necesarias para determinar definitivamente si las pendientes planas que se obtienen son debidas a un efecto de cuello de botella, o si los choques en la turbulencia supersónica previenen la formación de dicho efecto. Encontramos una notable similaridad entre el espectro de potencias de una onda explosiva MHD con el espectro de la componente irrotacional de la velocidad en turbulencia MHD, sugiriendo que la forma del espectro de potencias por si sola no prueba el dominio de una cascada turbulenta. Encontramos que hay relaciones sorprendentemente similares entre la media de las PDFs y el número de Mach para turbulencia hidrodinámica forzada y MHD de campo fuerte, aunque la relación tiene una gran dispersión. De esta forma, las PDFs de la densidad de masa no son una buena medida del campo magnético. Encontramos que las PDFs de turbulencia en decaimiento se desvían de la relación media-Mach obtenida para turbulencia forzada. Ésto implica que el número de Mach instantáneo por si sólo, no basta para determinar las propiedaes estadísticas de una turbulencia fuera de equilibrio. La dispersión respecto a la relación media-Mach para turbulencia forzada y el gran desvío de las PDFs para turbulencia en decaimiento respecto a la turbulencia forzada podrían ayudar a explicar la gran variación de eficiencia de formación estelar de nube a nube.

ABSTRACT

We present an analysis of velocity power spectra and probability distribution functions (PDFs) of the mass density in simulations of supersonic hydrodynamic and MHD turbulence with properties appropriate for molecular clouds. For this study we use Athena, a new higher-order Godunov code. We find that a resolution of 512^3 is insufficient to resolve an inertial range in the velocity power spectrum. Much higher resolutions will be necessary to determine definitively if the shallow slopes we find are due to a bottleneck effect, or if the shocks in supersonic turbulence prevent this feature from forming. We note a striking similarity between the power spectrum of an MHD blast wave with the power spectrum of the curl-free component of velocity in supersonic MHD turbulence, suggesting that the shape of the power spectrum alone does not prove the dominance of a turbulent cascade. We find there are surprisingly similar relationships between the mean of the PDF and the turbulent Mach number for driven hydrodynamic and strong-field MHD turbulence. There is, however, a large scatter about these relations. Thus, the PDF of the mass density is not a good measure of magnetic field strength. We find the PDF of decaying MHD turbulence deviates from the mean-Mach relation for the driven case. This implies that the instantaneous Mach number alone is not enough to determine the statistical properties of turbulence that is out of equilibrium. The scatter in the mean-Mach relation for driven turbulence and the large departure of decaying turbulence PDFs from those of driven turbulence may together help explain the large cloud-to-cloud variation in star formation efficiency.

Key Words: ISM: clouds — ISM: kinematics and dynamics — ISM: magnetic fields — simulations — stars: formation — turbulence

1. INTRODUCTION AND METHODS

We have numerically simulated supersonic hydrodynamic and MHD turbulence with properties appropriate for molecular clouds with the goal of

[1]Department of Astrophysical Sciences, Princeton University, Princeton, NJ 08544, USA.

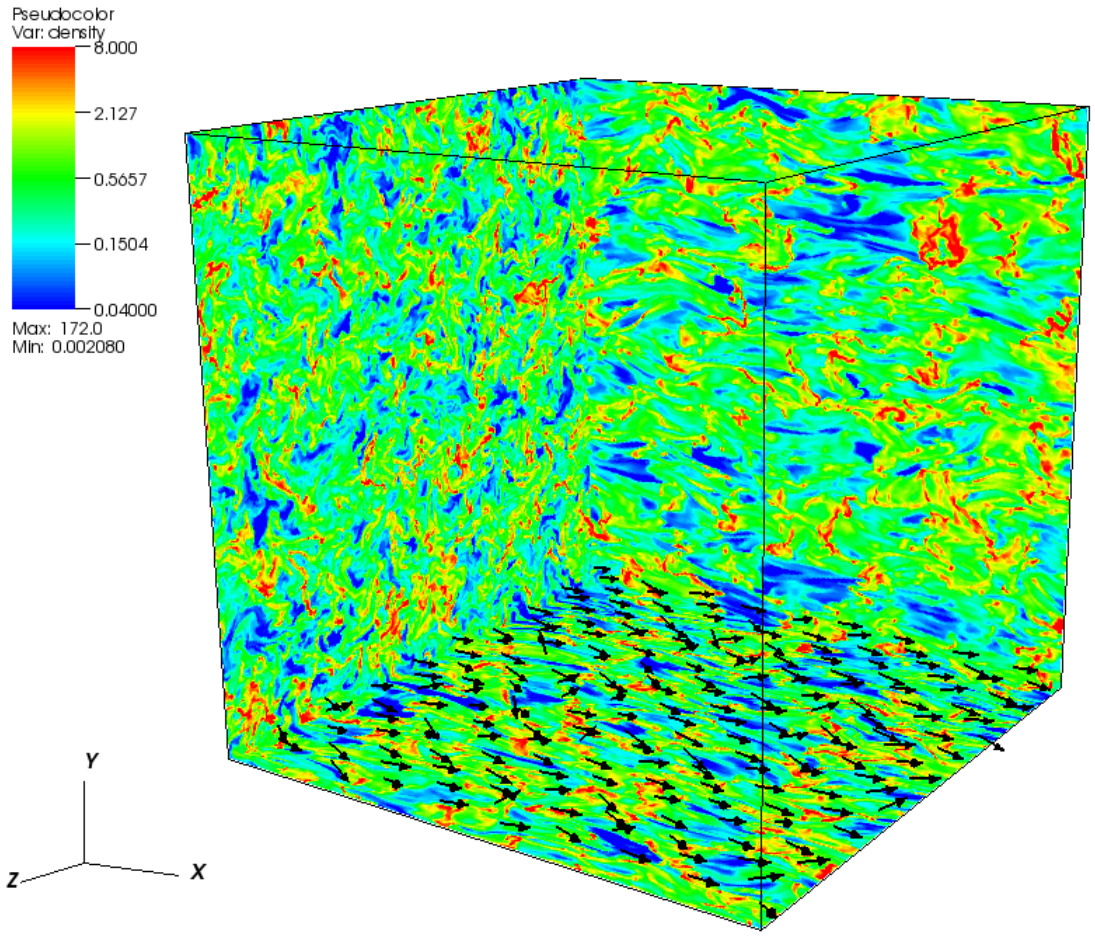

Fig. 1. Driven strong-field $\mathcal{M} \approx 5.4$ MHD turbulence with $k_{\rm pk}L/2\pi = 8$ at 512^3. Slices of density along the far faces of the cube on a logarithmic color scale from 0.04 (blue) to 8.0 (red). Magnetic field vectors along a slice normal to the y-axis at $y \approx 0.0645$ are fairly well aligned and there is anisotropy in the scale of the structures that results from the magnetic field.

better understanding the very early stages of star formation. These simulations were conducted at a resolution of 512^3 using the Athena code (Gardiner & Stone 2005; Stone et al. 2008; Stone & Gardiner 2008; Gardiner & Stone, in prep.) on a three-dimensional Cartesian grid of length $L = 1$ with periodic boundary conditions. Athena utilizes a higher-order Godunov scheme which exactly conserves mass, momentum, and magnetic flux. We solve the equations of ideal isothermal MHD,

$$\frac{\partial \rho}{\partial t} + \nabla \cdot (\rho \mathbf{v}) = 0\,, \tag{1}$$

$$\frac{\partial \rho \mathbf{v}}{\partial t} + \nabla \cdot (\rho \mathbf{v}\mathbf{v} - \mathbf{B}\mathbf{B} + P + B^2/2) = 0\,, \tag{2}$$

and

$$\frac{\partial \mathbf{B}}{\partial t} = \nabla \times (\mathbf{v} \times \mathbf{B})\,, \tag{3}$$

where $c_s = 1$ and $P = c_s^2 \rho$ are the isothermal sound speed and pressure, respectively. We use an approximate nonlinear Riemann solver (HLLD; Miyoshi & Kusano 2005) for our MHD runs and an exact nonlinear Riemann solver for our hydrodynamic runs. Both our MHD and hydro simulations are integrated well past the turbulent saturation time using a directionally-unsplit van Leer scheme (Stone & Gardiner 2008).

We initialize a uniform, stationary ambient medium with a mean density $\bar{\rho} = 1$ and magnetic field parallel to the x-axis whose amplitude B_0 is fixed by the value of $\beta = 2c_s^2\bar{\rho}/B_0^2$. We then apply divergence-free velocity perturbations following a Gaussian random distribution with a Fourier power spectrum of the form

$$|\delta \mathbf{v}_k^2| \propto k^6 \exp(-8k/k_{\rm pk})\,, \tag{4}$$

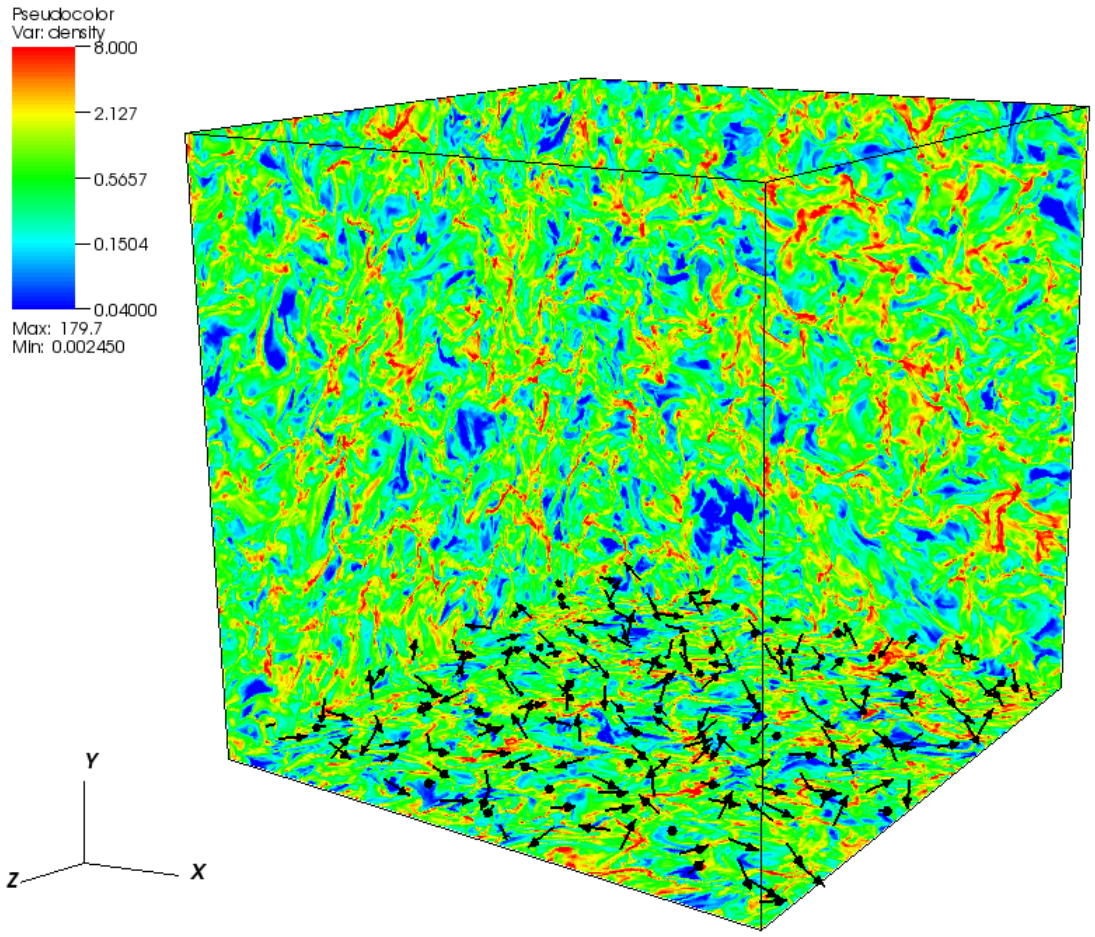

Fig. 2. Driven weak-field $\mathcal{M} \approx 5.3$ MHD turbulence with $k_{\rm pk}L/2\pi = 8$ at 512^3. Slices of density along the far faces of the cube on a logarithmic color scale from 0.04 (blue) to 8.0 (red). Magnetic field vectors along a slice normal to the y-axis at $y \approx 0.0645$ show much less alignment than in the strong-field case. The structures in this case are nearly isotropic.

for $kL/2\pi < N/2$, where N is the resolution and $k_{\rm pk}$ is the wavenumber of peak driving. Before applying the perturbations to the grid, we shift them such that no net momentum will be added and normalize them to give an energy injection rate $\dot{E}/\bar{\rho}L^2c_s^3$that yields roughly the desired turbulent Mach number in the saturated state. Energy is injected after each time step, with a new realization of the power spectrum generated at intervals $\Delta t c_s/L = 0.001$.

Figures 1 and 2 show slices in mass density along the far faces of the computational domain for driven strong-field ($\beta = 0.02$) and weak-field ($\beta = 2.0$) MHD turbulence, respectively, with the strongest driving at $k_{\rm pk}L/2\pi = 8$. Also included are magnetic field vectors in a slice normal to the y-axis near the bottom of the cube. Due to the strong background magnetic field, the vectors in Figure 1 are fairly well aligned. In Figure 2, however, the magnetic field vectors show less alignment with the background field. For both cases, the structure seen is filamentary. In the strong-field case, there is anisotropy in the scale of the structures as a result of the mean magnetic field. This is not to say, however, that the filaments are aligned with mean the magnetic field. In fact, some appear to be oriented perpendicular to the field.

Using simulations of this resolution, but driven at a larger scale, $k_{\rm pk}L/2\pi = 2$, we study the scaling of the velocity power spectrum with resolution for both hydrodynamic and strong-field MHD turbulence with Mach number $\mathcal{M} \sim 7$. Here we define the Mach number to be $\mathcal{M} \equiv \sigma_v/c_s$, where $\sigma_v = \langle v^2\rho/\bar{\rho}\rangle^{1/2}$ is the velocity dispersion of the gas, calculated using a mass-weighted average. We also investigate the scaling of the probability distribution function (PDF) of mass density with turbulent Mach

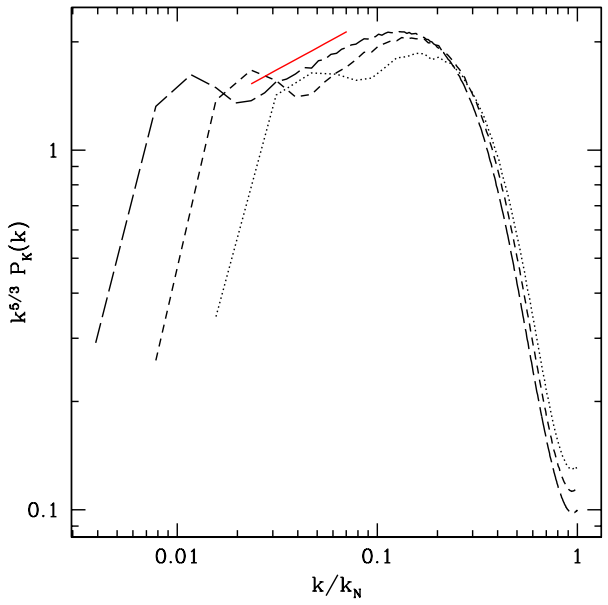

Fig. 3. Spherically-integrated compensated velocity power spectra for driven strong-field MHD turbulence runs with $k_{\rm pk}L/2\pi = 2$ at 512^3 (long dashed), 256^3 (dotted), and 128^3 (short dashed). The x-axis has been renormalized to give $k/k_N = 1$. Also shown is a fit (solid) to the slope of the 512^3 run over the range $6 \le kL/2\pi \le 18$, $P(k) \propto k^{-1.36}$.

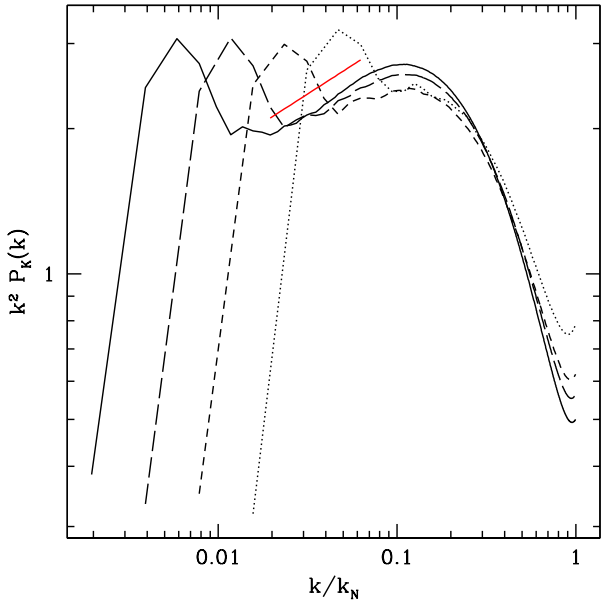

Fig. 4. Spherically-integrated compensated velocity power spectra for driven hydro turbulence runs with $k_{\rm pk}L/2\pi = 2$ at 1024^3 (solid), 512^3 (long dashed), 256^3 (dotted), and 128^3 (short dashed). The x-axis has been renormalized to give $k/k_N = 1$. Also shown is a fit (solid) to the slope of the 1024^3 run over the range $10 \le kL/2\pi \le 32$, $P(k) \propto k^{-1.76}$.

number to infer the amount of high-density material in the cloud. This will allow us to infer the amount of high-density material that will be available to form the bound clumps that will eventually collapse to form stars.

2. POWER SPECTRA

Figure 3 shows the compensated velocity power spectrum for driven strong-field MHD turbulence with $\mathcal{M} \sim 7$. By compensated, we mean that we have multiplied the power spectrum by a power law in order to make the inertial range appear more horizontal. This has the advantage of making small deviations from a power law very obvious, but one should keep in mind that it greatly distorts the high wavenumber end of the spectrum. At our highest resolution, we find a much shallower slope, $P(k) \propto k^{-1.36}$, than would generally be expected by researchers in the field. Our power spectrum of the quantity $\mathbf{u} = \rho^{1/3}\mathbf{v}$ also shows a very shallow slope. Most would blame this on the bottleneck effect, a build-up of power at small scales, commonly seen in subsonic turbulence, due to the low levels of numerical dissipation inherent to this type of numerical method. It is not clear, however, that any power that might build up at small scales would not be easily dissipated by shocks in supersonic turbulence. Significantly higher resolutions, which are currently out of reach, will be required in order to definitively identify the inertial range in the power spectrum.

Figure 4 shows the compensated velocity power spectrum of driven hydrodynamic turbulence, also at $\mathcal{M} \sim 7$. At our highest resolution of 1024^3, we find $P(k) \propto k^{-1.76}$, again shallower than expected. There may be a short range with steeper slope starting to appear, but at this resolution it appears to be even steeper than k^{-2}. Again, significantly higher resolutions will be necessary to gain a clear understanding of what we are seeing.

The power law slope of the velocity power spectrum is often taken to be evidence that a turbulent cascade, similar to the one characteristic of incompressible turbulence, dominates supersonic turbulence as well. Unlike in incompressible turbulence, however, energy at any scale in highly-compressible turbulence can be dissipated in shocks. To understand how tight a constraint the power spectrum puts on the relative importance of shocks, in Figure 5 we compare the power spectrum of an MHD blast wave to that of our $\mathcal{M} \sim 7$ MHD turbulence, both at 256^3. We find the velocity power spectrum

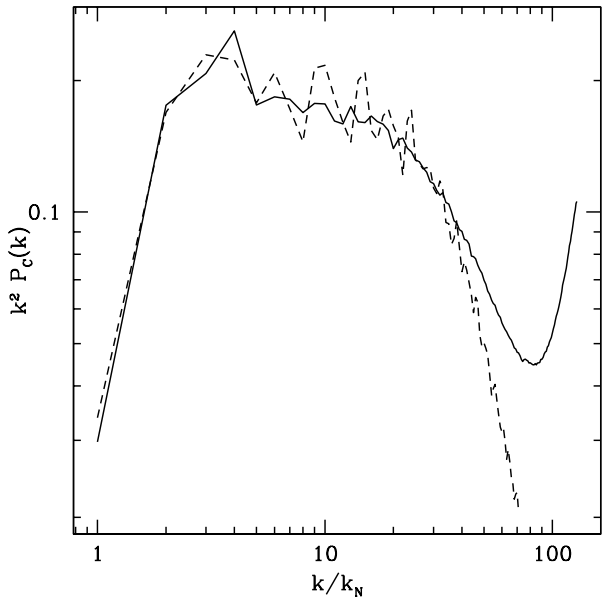

Fig. 5. Spherically-integrated compensated power spectrum of the curl-free component of velocity from one snapshot of the 256^3 driven strong-field MHD turbulence run (solid) shown in Figure 3, compared to the total velocity power spectrum of a spherical MHD blast wave (short dashed), also at 256^3. Except for the oscillations, the shapes of these spectra look quite similar between the driving and dissipative scales.

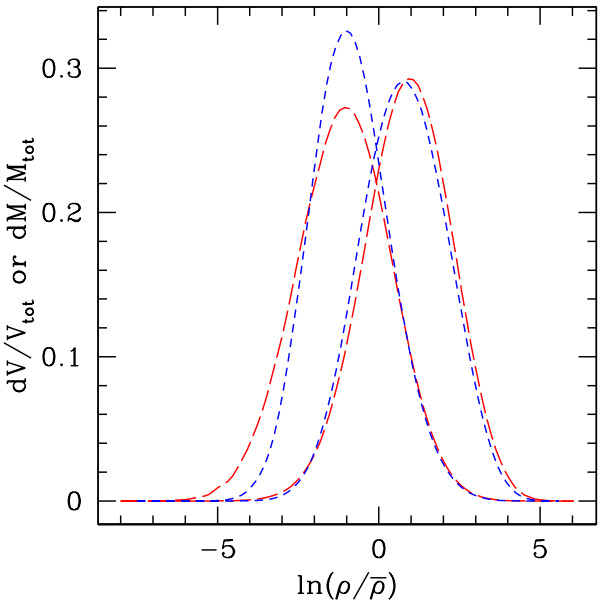

Fig. 6. Probability distribution functions of the logaritm of density for driven hydrodynamic (red long dashed) and strong-field MHD (blue short dashed) turbulence.

of the blast wave to be quite similar to the power spectrum of the curl-free component of velocity in MHD turbulence. As we should expect, the power spectrum of a shock or blast wave (any discontinuity) will have $P(k) \propto k^{-2}$. It would seem that the shape of the power spectrum alone does not rule out shocks as playing a significant role in supersonic turbulence. Other diagnostics, such as structure functions, may prove to be more useful in this regard.

3. PROBABILITY DISTRIBUTION FUNCTIONS

Turbulence in molecular clouds causes converging flows where the gas can be compressed to very high densities. The PDF of the density tells us the fraction of the mass or volume that falls within a given density range. Although most of the volume of the cloud is at below-average density, the majority of the mass is found at above-average density. Since self-gravitating clumps can form in the high-density regions, understanding PDFs is critical for understanding the stellar IMF and SFR.

If compression and rarefaction events in the turbulent gas within a molecular cloud are spatially and temporally independent, the PDF of density will have a log-normal distribution (Passot & Vazquez-Semadeni 1998). The PDF of the logarithm of density, then, will have a normal distribution given by

$$f(y)dy = \frac{1}{\sqrt{2\pi\sigma^2}} \exp\left[\frac{-(y+\mu)^2}{2\sigma^2}\right] dy\,, \qquad (5)$$

where $y \equiv \ln(\rho/\bar{\rho})$, μ is the mean of the distribution, and σ^2 is the dispersion, with $|\mu| = \sigma^2/2$. Our goal is to analyze the relationship between the mean of the distribution and the turbulent Mach number of the cloud. This mean will be representative of the median density within the cloud.

Figure 6 shows time-averaged PDFs of $\ln\rho$ for both hydrodynamic and MHD turbulence, which do in fact approximate Gaussian distributions. The two curves that peak at negative values of $\ln\rho$ represent the fraction of the cloud's *volume* that falls within a given density range. The two curves that peak at positive values, on the other hand, are the fraction of the cloud's *mass* that falls within a given density range. This is the case because, although most of the cloud's mass is within high-density clumps, most of the cloud's volume is in the low-density regions.

3.1. *Time-averaged Mean-Mach Relation*

We have investigated the relation between the mean of the PDF and the turbulent Mach number over a range of Mach numbers $1.2 \leq \mathcal{M} \leq 7.0$ for both driven hydrodynamic and driven strong-field MHD turbulence. We found that a resolution of 512^3

gave smoother-looking PDFs which could be fit more accurately than those from 256^3 simulations, justifying the computational expense. Higher resolution also allows us to study scatter in the PDF in subvolumes of the domain. To minimize the effects of intermittency, we time-average the PDFs obtained from seven snapshots in the saturated state spanning almost 3 dynamical times before fitting them.

Since the tails of the PDFs will deviate from normal form due to the effects of intermittency, we fit only bins with values of at least 10% of the peak value. We perform a Levenberg-Marquardt least-squares fit with uniform weighting. Once we have obtained the mean, μ, of the best-fit distribution, we plot it against a function of turbulent Mach number, $\xi(\mathcal{M}) = \ln[1+\alpha\mathcal{M}^2]$. With the appropriate choice of α, we can obtain a linear relation between the PDF mean and this function, $\xi(\mathcal{M})$.

Figure 7 shows the mean-Mach relation found from time-averaged PDFs over the full domain for both driven hydrodynamic and MHD turbulence. We find that a value of $\alpha = 0.5$ in the function $\xi(\mathcal{M})$ gives the best linear relations. In the hydro case, for the volume fraction we find

$$\mu_V = -0.36 \ln[1 + 0.5\mathcal{M}^2] + 0.10\,, \qquad (6)$$

while for the mass fraction we find

$$\mu_M = 0.32 \ln[1 + 0.5\mathcal{M}^2] - 0.10\,. \qquad (7)$$

Because the density fluctuations in subsonic turbulence are not produced by shocks, we have no reason to expect these relations to approach zero with turbulent Mach number. The mean-Mach pairs from the time-averaged PDFs fall very close to these relations. Over the full range of Mach numbers tested, however, the time-averaged means are smaller than those found by Padoan et al. (1997), $\mu_{V,M} = \mp 0.5 \ln[1 + 0.25\mathcal{M}^2]$. To determine the magnitude of the effect that the driving may have had on the relations, we also compare values determined from hydrodynamic turbulence with $k_{\rm pk}L/2\pi = 4$ (not shown), finding that these points fall very close to the $k_{\rm pk}L/2\pi = 2$ relations as well. For the MHD case, we find

$$\mu_V = -0.29 \ln[1 + 0.5\mathcal{M}^2] - 0.06\,, \qquad (8)$$

for the volume fraction and

$$\mu_M = 0.28 \ln[1 + 0.5\mathcal{M}^2] + 0.07\,, \qquad (9)$$

for the mass fraction, still yielding means smaller than those found by P97.

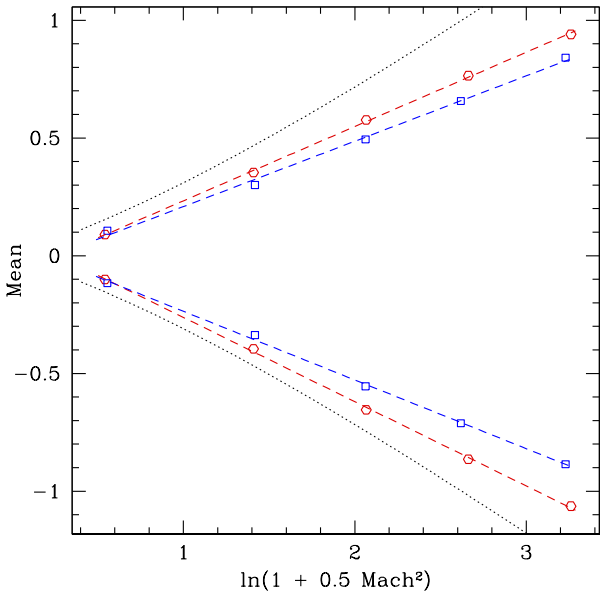

Fig. 7. PDF means versus $\xi(\mathcal{M})$ for driven hydro (red hexagons) and strong-field MHD (blue squares) turbulence. Also shown are the fitted mean-Mach relations for hydro (red dashed) and MHD (blue dashed). For comparison, the relation from Padoan et al. (1997) is shown as well (black dotted).

3.2. *Scatter in the Relation*

Observations show a wide range of star formation rates for different clouds. To infer from our simulations the level of cloud-to-cloud variation we would likely observe, we also investigate the mean-Mach relation for regions of size comparable to the driving scale. To do this, we divide our computational domain into eight equal sub-domains, each of resolution 256^3. We compute the PDF in each of these sub-boxes (which we will refer to as sub-PDFs) individually and plot their means against the turbulent Mach number within that sub-box.

We compute our sub-PDFs using the velocity dispersion and mean density in the sub-box instead of over the global domain. We do not time-average our results, yielding 56 mean-Mach pairs for each run. Although the snapshots are at intervals of just under half a dynamical time on the global scale, the interval between snapshots is closer to a flow crossing time on the scale of the sub-boxes, making them sufficiently uncorrelated for this analysis. Substantial scatter in the values within a run might help explain the observed cloud-to-cloud variation in the star formation rate in molecular clouds.

Figure 8 includes the time-averaged mean-Mach relation presented in Figure 7 as well as the instan-

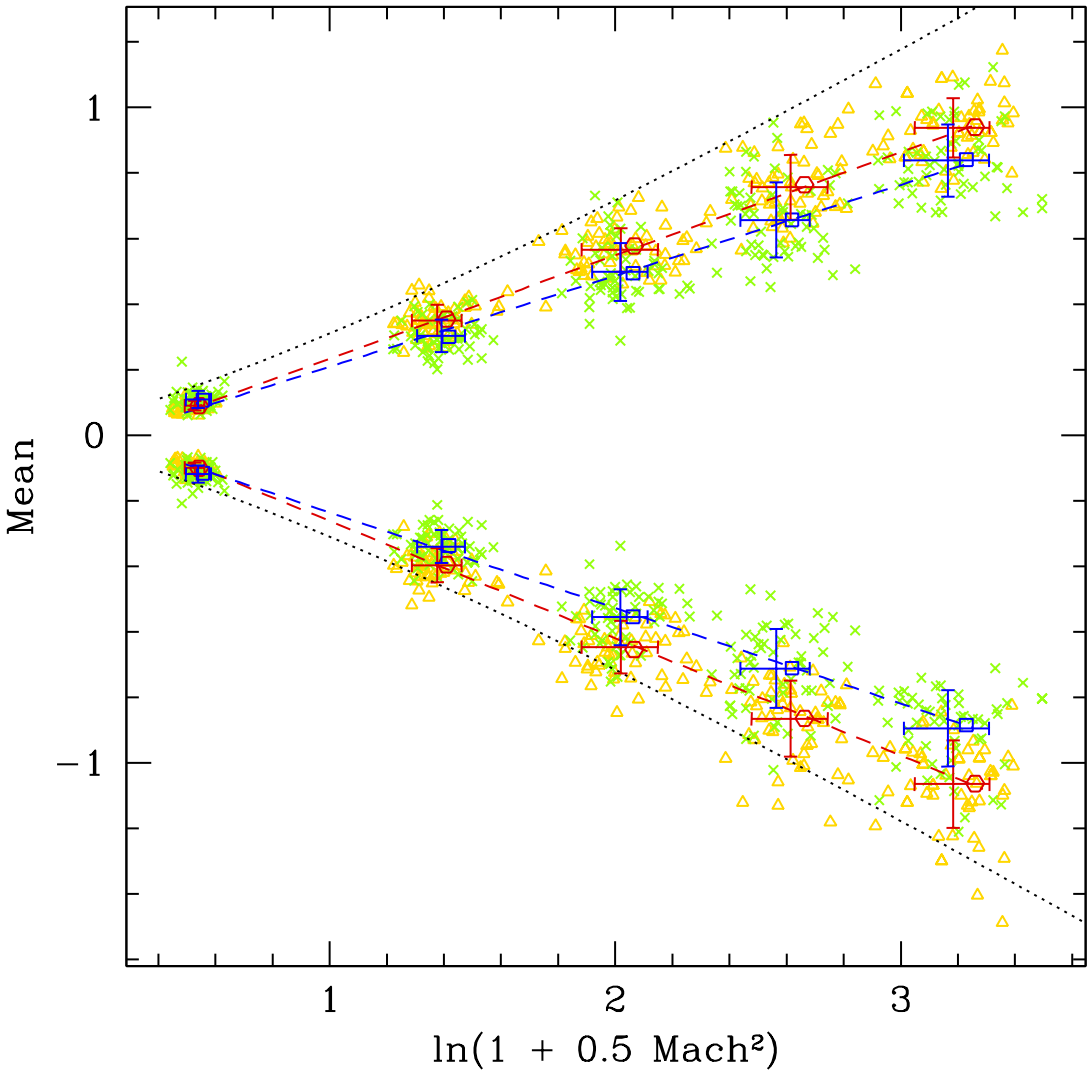

Fig. 8. PDF means versus $\xi(\mathcal{M})$ for driven hydro (red hexagons) and strong-field MHD (blue squares) turbulence. Only time-averaged PDFs over the full domain are used to fit the mean-Mach relation (hydro: red dashed; MHD: blue dashed). Also shown are the instantaneous values taken from each of the eight driving-scale sub-boxes (hydro: gold triangles; MHD: green crosses) and the 1σ error bars on those points (hydro: red; MHD: blue). For comparison, the relation from Padoan et al. (1997) is also shown (black dotted).

taneous mean-Mach pairs found from each of the eight sub-boxes for both hydrodynamic and MHD turbulence. The scatter in these points, illustrated by 1σ error bars on the plot, is quite significant. The average of all 56 points for each run falls at a slightly lower Mach number than the value found from the time-average over the full domain since the Mach number typically decreases on smaller scales. These averages also differ slightly from those computed from time-averaged full-domain PDFs, due to reversing the order of averaging and fitting, although they still fall close to the relation found. The 1σ scatter in the Mach number is 4–8%, while in the sub-PDF means it is 16–17% for the lowest Mach number run and 10–14% for the remaining runs. This scatter puts some of the instantaneous sub-PDF values in the vicinity of the P97 relation.

The instantaneous mean-Mach pairs found from sub-boxes have even more scatter for the MHD case than for the hydro case. The 1σ scatter in the Mach number is 5–8%, while for the sub-PDF means it is 22–24% for the lowest Mach number run and 13–18% for the remaining runs. Although the relations found for hydro and MHD differ, the sub-PDF values

overlap substantially, making them difficult to distinguish observationally. The relations found from the time-averaged values over the full domain fall a bit less than 1σ apart.

3.3. *Assumption of Equilibrium*

We have shown in the previous two sections that there is a large scatter about the mean-Mach relation for driven turbulence, both with and without a magnetic field. As it seems likely that molecular clouds are transient entities, however, it may be more appropriate to study decaying turbulence. We now compare one decaying MHD turbulence run (non-equilibrium) to our mean-Mach relation found from multiple driven (equilibrium) runs.

The decaying run, shown in Figure 9, is initialized from a snapshot of fully-developed turbulence from our highest Mach number driven run. Although this snapshot has a full-domain PDF mean roughly 1σ more extreme than the time-averaged driven relations, this should not affect the results. The arrow of time for this decaying turbulence simulation runs from right to left in the plot. At first the small change in mean as the Mach number decreases causes a shallower slope than that of the driven relation. Once the mean begins to change appreciably, however, the slope becomes much steeper, crossing the driven relation at roughly $\mathcal{M} = 4.5$. Although the slope shallows some as low Mach numbers are reached, it remains steeper than the driven relation for as long as we follow it.

The evolution of this decaying run does not parallel or asymptotically approach the driven relation at the same magnetic β. Contrary to what was found by Passot & Vazquez-Semadeni (1998) for one-dimensional polytropic gas, then, we find that the instantaneous Mach number is insufficient to describe the properties of the turbulent medium when the gas is not in a statistically steady state. This is consistent with the findings of Ostriker et al. (2001) for the PDFs of decaying turbulence. If MCs contain decaying turbulence, which seems likely (Heitsch et al. 2006), the PDF may be "out of equilibrium", making relations obtained from steady state (driven) turbulence inapplicable.

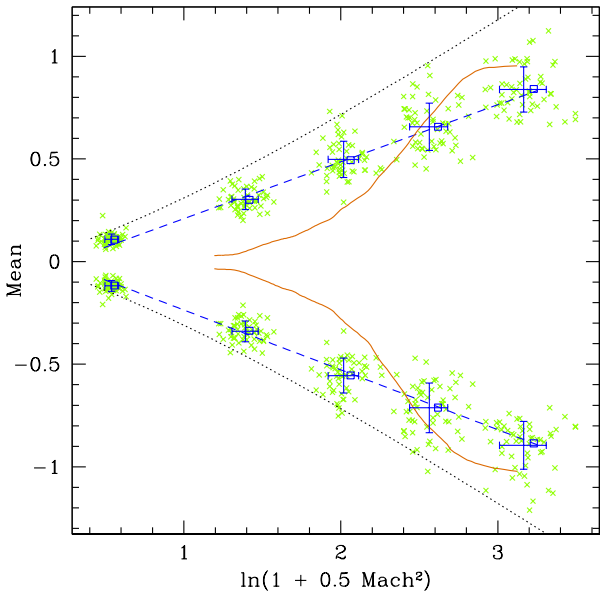

Fig. 9. PDF means versus $\xi(\mathcal{M})$ for decaying MHD turbulence (orange solid), contrasted with the driven values (blue squares) and relation found in § 3.1 (blue dashed). Also shown are the driven sub-PDF values (green crosses) and 1σ error bars. The decaying run does not follow the relation found for driven MHD, even considering the large scatter found in the driven sub-PDFs. For comparison, the relation from Padoan et al. (1997) is also shown (black dotted).

4. DISCUSSION AND CONCLUSIONS

We find from our velocity power spectra that a resolution of 512^3 is insufficient to definitively resolve an inertial range. The slopes of our power spectra are shallower than most results reported in the literature, however our insufficient resolution prevents us from determining the cause. The spherically-averaged power spectrum of the curl-free component of velocity in driven MHD turbulence approximates the velocity spectrum of an MHD blast wave. This suggests that the shape of the spectrum alone is not evidence of a turbulent cascade. It is possible that shocks play a significant role in the regulation of energy transfer between spatial scales in supersonic turbulence. The analysis of structure functions may be useful in distinguishing a turbulent cascade from dissipation by an ensemble of shocks.

We have found there is a one-to-one-correspondence between the mean of the time-averaged PDF and the turbulent Mach number for both hydrodynamic and strong-field MHD turbulence. The mean-Mach pairs from the time-averaged PDFs fall very close to these relations, but have smaller PDF means for a given Mach number than were found by Padoan et al. (1997) for the purely hydrodynamic case. By also investigating the instantaneous PDFs in sub-volumes, we have found a large scatter about the time-averaged mean-Mach relation. The scatter found from the sub-PDFs could help explain the large variation

in the observed SFR in MCs. Due to the large scatter about the mean-Mach relation, there is insufficient difference between hydrodynamic and MHD turbulence for this to be a useful diagnostic for distinguishing between the two observationally. For the strong-field MHD case, the means from the time-averaged PDFs over the full domain are only roughly 1σ smaller than the corresponding hydrodynamic values.

We have also compared the relation between PDF mean and turbulent Mach number for decaying MHD turbulence to that of the driven case. We find that our driven mean-Mach relation does not hold for decaying MHD turbulence at the same magnetic β. It would seem that the instantaneous Mach number in decaying turbulence does not adequately describe the statistical state of the turbulent gas. Since molecular clouds are likely to be transient entities, relations found from driven turbulence may not be applicable to real clouds. Since there is overlap between the driven and decaying values for some Mach numbers, this information can not be used to distinguish between driven and decaying turbulence.

A more detailed analysis of energy dissipation, power spectra, PDFs, and intermittency can be found in forthcoming papers (Lemaster & Stone 2008, 2009).

We thank Eve Ostriker for very productive discussion. Simulations were performed on the IBM Blue Gene at Princeton and on computational facilities supported by NSF grant AST-0216105.

REFERENCES

Gardiner, T. A., & Stone, J. M. 2005, J. Comput. Phys., 205, 509
Heitsch, F., et al, 2006, ApJ, 648, 1052
Lemaster, M. N., & Stone, J. M. 2008, ApJ, 682, L97
_____. 2009, ApJ, 691, L1092
Miyoshi, T., & Kusano, K. 2005, J. Comput. Phys., 315, 344
Ostriker, E. C., Stone, J. M., & Gammie, C. F. 2001, ApJ, 546, 980
Padoan, P., Jones, B. J. T., & Nordlund, A. P. 1997, ApJ, 474, 730
Passot, T., & Vazquez-Semadeni, E. 1998, Phys. Rev. E, 58, 4501
Stone, J.M., & Gardiner, T.A. 2009, NewA, 14, 139
Stone, J.M. et al. 2008, ApJS, 178, 137